

ORIGINAL RESEARCH PAPER

Numerical Analysis of Surface Potential Change on Electroosmotic Flow in a Microchannel with Using Density-Based WCSPH

Mojtaba Dehghanzadeh Bafghi¹, Mohammad Sefid^{1*}, Rahim Shamsoddin², A. M. Salehizadeh³

¹Energy Conversion Department, Mechanical Engineering Faculty, Yazd University, Yazd, Iran.

²Energy Conversion Department, Mechanical Engineering Faculty, Sirjan University, Sirjan, Iran.

³Applied Design Department, Mechanical Engineering Faculty, Yazd University, Yazd, Iran

Received 9 April 2021;

revised 4 February 2022;

accepted 12 February 2022;

ABSTRACT: We investigate the phenomenon of electrokinetics in microchannels. Electroosmotic is one of the four electrokinetic effects. Electroosmotic flow (EOF) is caused by the application of an electric field to an aqueous solution. The characteristics of the EOF depend on the nature of the surface potential distribution. EOF in microfluidic systems is limited to low Reynolds. As a result, species mixing in EOF systems is primarily due to diffusion. The surface heterogeneous of the microchannel walls causes the production of micro vortexes in the liquid. In this study, A two-dimensional microchannel is used to study the electroosmotic/pressure driven in Newtonian fluids. The equations governing the fluid flow in a rectangular microchannel are obtained based on the Lagrangian approach and using the density-based weakly compressible smoothed particle hydrodynamics (WCSPH) method. We have analyzed the vortexes due to surface potential heterogeneity and investigated increasing the surface potential on the flow. The results show that increasing the surface potential causes the vortexes to grow and strengthens the velocity and mixing fields more.

KEYWORDS: *Electroosmotic flow, Smooth particle hydrodynamics, Rectangular microchannels*

INTRODUCTION

The electroosmotic phenomenon is crucial in the design and understanding of concepts such as reagents for laboratory chip systems and the analysis of biological systems. Because the reactions associated with these Microchannels have been widely used in various areas of chemistry and biochemistry. In such microfluidic systems, electroosmosis is utilized as the tool for fluid transport and species mixing. The Reynolds number of EOFs is minimal, and achieving sufficient mixing in electroosmotic microchannel flow can be difficult. In general, microchannels are divided into active and inactive categories to increase mixing [1]. Passive micromixers usually use different geometric shapes to increase the contact surface of the mixed liquids, and the main problem with passive mixing is the complexity of microscale fabrication. In contrast to passive mixers, active mixers, by removing the moving parts inside the microchannels, stir the flow stream by applying an external pressure perturbation or an electric field.

Preliminary previous studies have focused on EOF with uniform surface electric potential ψ or zeta potential ζ . Dutta and Beskok [3] presented an analytical solution for the EOF for uniform surface electric potential.

*Corresponding Author Email: mhsefid@yazd.ac.ir

Tel.: +989133505702; Note. This manuscript was submitted on April 9, 2021; approved on February 4.

They obtained analytical solutions for the fluid velocity, pressure and shear stress using the modified momentum equation. Hu and Chao [4] investigated both numerical and experimental performance of the electroosmotic pump. Patankar and Hu [5] developed a numerical program to study the EOF in a microchannel. Furthermore, many other studies were done in the field of uniform surface potential.

The effects of nonuniform surface potential distributions on EOFs have been examined by several researchers. Ajdari et al. [6] investigated the phenomenon of electroosmosis with nonuniform surface potential. They found that rotational zones by applying the surface potential opposite to the surface charge were created. Ren et al. [7] investigated the EOF in circular microchannels by changing the axial pitch of the surface potential and observed perturbation velocity profiles in the flow. Erickson and Li [8] investigated the rotational regions in the flow in T-shaped micromixers with nonuniform surface potentials. They found that the rotation region is more significant, and more robust, when the potential for a heterogeneous surface is equal to and opposite to a homogeneous surface. The velocity and potential distributions near the jump site in the surface potential have been analytically investigated by Yariv [9]. Tian et al. [10] observed that excellent mixing through

Nomenclature	
B, \hat{B}	Corrective tensor
c_0	Completely unmixed Concentration (molem ⁻³)
c_∞	Completely mixed Concentration (molem ⁻³)
c	Concentration (molem ⁻³)
C	Sound velocity (ms ⁻¹)
D	Mass diffusion coefficient (m ² s ⁻¹)
e	Elementary electric charge (c)
e_{ij}	Unit vector
E_0	External electric field (Vm ⁻¹)
f	Scalar function
F	Vector function
g	Gravity acceleration (ms ⁻²)
G	Relative position vector function
h	smooth length (m)
H	Half the height of the microchannel (m)
k_b	Boltzmann constant (Jk ⁻¹)
L	The length of the microchannel (m)
n_∞	bulk ionic number concentration (m ⁻³)
P, P_0	Pressure and Reference pressure (kgm ⁻¹ s ⁻²)
r	Position vectors (m)
Re_{ref}	Reference reynolds
T	Absolute temperature (K)
u	Velocity component in x-direction (ms ⁻¹)
U	Dimensional horizontal velocity (ms ⁻¹)
U_{ref}	Reference velocity (ms ⁻¹)
v	Velocity component in y-direction (ms ⁻¹)
V	Velocity vector (ms ⁻¹)
\tilde{V}	Middle mean velocity (ms ⁻¹)
W	Kernel function
z	valance
Greek Letters	
ϵ_r	dielectric constants of the solution
ϵ_0	Permittivity of vacuum (Fm ⁻¹)
Z	Zeta potential (v)
η	Vertical dimensionless length
λ_D	Debye length
λ_D^{-1}	Debye–Huckel parameter
μ	Dynamic viscosity (kgm ⁻¹ s ⁻¹)
ν	kinematic viscosity (m ² s ⁻¹)
ξ	Horizontal dimensionless length
ρ, ρ_0	Density and Refrence density (kgm ⁻³)
ρ_f	Free charge density (Cm ⁻³)
σ	Mixing efficiency
Φ	total potential (v)
φ	External electrical potential (v)
ψ	potential of the electric double layer (v)
ω	particle volume (m ³)
Superscripts	
*	Dimensional values
n	Time step
Subscripts	
in	Inlet values
i, j	Particle counter
k	Repeat step counter
out	outlet values

nonuniform surface potential in microchannels might lead to inferior mass transfer. Lee et al. [11] analyzed the EOF with nonuniform potential in a microchannel assuming zero volumetric electric force outside the electric double layer (EDL). The time-dependent EOF distributed by an alternating flow electric field with surface potential heterogeneity along the microchannel walls was investigated by Luo [12]. Bhattacharyya and Nayak [13] showed that the patch potential might increase the mixing of liquids in microchannels. Bhattacharyya and Nayak [14] found that surface geometry changes and surface potential heterogeneity cause more intense convection effects in nanochannels.

Using experimental methods, Sun and Shie [15] experimentally investigated the performance of divergent intra-microchannel mixing under EOFs with periodic potential and identified the optimal phase difference and the optimal half-angle of divergence for the best mixing performance. Jain and Nandakumar [16] have used the numerical optimization methods to study different geometry formulations with different load patterns and for each case, have shown the optimal load pattern for the maximum mixing rate. Sadeghi et al. [17] studied heat transfer in EOFs with excitation pressure and found that when the ratio of

width to height of the channel increases, the Nusselt number generally increases. Cheng et al. [18] simulated electroosmotic mixing with periodic potentials using the Helmholtz-Smolokowski model and concluded that vortices induced by EOFs increase the quality of mixing at low frequencies while at the same frequency, high mixing is reduced. Gaikwad et al. [19] analyzed the entropy generation in electroosmotic-pressure driven flows for the microchannel. It was reported that enhanced velocity gradients lead to a more entropy generation rate. Azari et al. [20] developed some expressions for the velocity distribution and temperature distribution for the microchannels in the electroosmotic pressure driven flows. Their results showed that the EDL thickness affects the velocity and Nusselt number. Kazemi et al. [21] used a numerical method to investigate the effect of placing a conductive flap inside the channel on the mixing performance and significant mixing has been reported. They used the simple Helmholtz Smolokowski model for their simulation. Sheikhizad and Kalteh [22] illustrated electroosmotic and pressure driven Newtonian nanofluid flow in a microchannel via Lattice Poisson-Boltzmann method. They investigated effects of different parameters such as surface potential and slip coefficient on flow filed. They found out increasing the slip

coefficient causes the velocity enhancement in the EOF and heterogeneous surface potential moves the vortices toward the walls. Qaderi et al. [23] performed micro-mixing of the combined electroosmotic-pressure driven flow inside the microchannels with the triangular obstacles (hurdles) and heterogeneous zeta-potential. The results showed that for the straight homogeneous microchannels, greater adverse pressure gradients cause better mixing. Microchannels having the hurdles or heterogeneous zeta potential produce the superior mixing performance.

In this research, the electrokinetic micropump has been investigated. Electrokinetic micropumps can be associated with pressure gradients, in which case they are referred to as electroosmotic / pressure driven micropumps, or they can be caused only by electrokinetic effects. In this paper, the numerical code is based on the density-based WCSPH. Most of the studies used the network method and few studies focused on the Lagrangian approach of EOFs. Also, the presence of the hyperbolic sine term in Poisson-Boltzmann equation has made this equation extremely unstable. Using SPH method, we have eliminated these instabilities. In addition, for fast mixing processes, the SPH method provides more stable and accurate solutions than the based- mesh methods. Therefore, the EOFs are modeled by using the density-based WCSPH method. One of the most important issues in microsystems is mixing. In order to achieve better mixing, the effect of increasing the zeta potential has been investigated. This modeling technique shows this effect on the flow pattern.

FORMULATION

Electric double layer

By placing the charged surface in the vicinity of the electrolyte solution, the surface reaction between the electrolyte ions and the adjacent surface causes the surface to become charged. The forces of attraction and repulsion between surface charges and the electrolyte change the arrangement of ions within the electrolyte, and eventually, a region called the EDL is formed near the surface. In other words, the charged dielectric surface forms this region by absorbing ions opposite to its charge. As a result, there is a distribution of ions opposite the surface charge in the electric double region, while outside the electrolyte region is neutral (free from charge). By applying an external electric field on this EDL, a force is applied to the charges in this layer, and this force causes the ions to move to cause the fluid flow in the electric double layer. Finally, due to friction between the fluid layers, even the outer fluid flows from the electric double layer. This type of flow is called EOF. The distribution of the electric potential in the solution due to double electric layer ψ is described by the Poisson-Boltzmann equation [25].

$$\nabla^2 \psi = \frac{-\rho_f}{\epsilon_0 \epsilon_r} \quad (1)$$

Where the ψ potentials of the EDL, ϵ_r and ϵ_0 represent the dielectric constants of the solution and in vacuum, respectively. ρ_f is the free charge density is given [25].

$$\rho_f = ze(n_+ - n_-) \quad (2)$$

n_+ and n_- show the concentration of positive and negative ions, z represents the valance and e represents electron charge. The charge density can be expressed in terms of the Boltzmann distribution, which for a symmetric solution $n_+ = n_- = n$ using the Boltzmann distribution for ionic concentration [25]:

$$\rho_f = -2zen_\infty \sinh\left(\frac{ze\psi}{k_b T}\right) \quad (3)$$

Where n_∞ is bulk ionic concentration, z is the ionic capacity, k_b is the Boltzmann constant, T is the absolute temperature. By placing equation (2) in equation (1) and using the Boltzmann distribution for the ionic species, the well-known Poisson-Boltzmann equation is obtained as follows [25]:

$$\frac{\partial^2 \psi}{\partial x^2} + \frac{\partial^2 \psi}{\partial y^2} = \frac{2zen_\infty}{\epsilon_0 \epsilon_r} \sinh\left(-\frac{ze\psi}{k_b T}\right) \quad (4)$$

The thickness of the EDL is approximated by the debye length of λ_D . The Debye length is a characteristic of the electrolyte solution and depends on the molar concentration of the fluid, and its thickness can be estimated by the Debye-Huckel parameter λ_D^{-1} [25].

$$\lambda_D^{-1} = \frac{1}{\lambda_D} = \left[\frac{2z^2 e^2 n_\infty}{\epsilon_0 \epsilon_r k_B T} \right]^{1/2} \quad (5)$$

In EOFs, the main idea is that by applying an external electric field such as φ to the electric charge of the EDL, the existing electrolyte can be moved. The application of this external electric field to a charged fluid results in the creation of a pure electric force $\rho_f E_0$, which is called the Lorentz force, in which E_0 is the external electric field strength $E_0 = \partial\varphi/\partial x$. The potential of an applied electric field φ is obtained by solving the Laplace equation [25].

$$\nabla^2 \varphi = 0 \quad (6)$$

Conservation and constitutive equations

When an electric current is applied the EDL. EOF is obtained. Two-dimensional, incompressible, and laminar flow is intended for a Newtonian fluid. Most of the electrolytes used in the electroosmotic flow behave like Newtonian fluid, so the fluid here is considered Newtonian. The governing equations are the mass conservation equation, the momentum equation, the state equation and the concentration equation, respectively. The Navier-Stokes equations can be used in flow analysis, because the mean free molecular path is from the Angstrom order, a continuum

flow regime is assumed. In this case, the Knudsen number is in the range of the continuum flow regime.

$$\frac{d\rho}{dt} = -\rho \nabla \cdot V \quad (7)$$

$$\rho \frac{dV}{dt} = \mu \nabla^2 V + \rho g - \nabla P + \rho_f E \quad (8)$$

$$P - P_0 = C^2(\rho - \rho_0) \quad (9)$$

$$\frac{dc}{dt} = D \nabla^2 c \quad (10)$$

In equations 9-12, ρ is the density, V is the velocity, P is the pressure, g is the gravitational acceleration, μ is the viscosity of the fluid, D is the mass diffusion coefficient, c is the concentration and C is the sound velocity, and d represents the material derivative. $\rho_f E$ is the volumetric force caused by the application of an electric field acting on a fluid equal to [25]:

$$E = -\nabla \Phi \quad (11)$$

Where Φ is the total potential due to the linear sum of the potential of the EDL ψ and the potential of the applied electric field φ (i.e. $\Phi = \psi + \varphi$).

In order to evaluate the mixing quality, the mixing efficiency is defined, which shows the Mixing efficiency at each cross section of the microchannel and is defined as follows [25].

$$\sigma(x) = \left(1 - \frac{\int_{-H}^{+H} |c - c_\infty| dy}{\int_{-H}^{+H} |c_0 - c_\infty| dy} \right) \quad (12)$$

Where c_0 and c_∞ are the concentrations of the species not fully mixed and completely mixed, respectively.

Boundary conditions

To solve the Poisson-Boltzmann equation, the potential flux at the input and output is assumed to be zero.

$$\begin{cases} \text{inlet } x = 0 & \partial\psi/\partial x = 0 \\ \text{outlet } x = L & \partial\psi/\partial x = 0 \end{cases} \quad (13)$$

And the pattern of zeta potential distribution on the microchannel wall is (as shown in Fig. 1):

$$\begin{cases} y = H & \psi = \zeta(x) \\ y = -H & \psi = -\zeta(x) \end{cases} \quad (14)$$

The Laplace equation is solved with the following boundary conditions. A constant potential φ_{in} is given at the inlet of the channel and a constant potential φ_{out} at the channel's outlet is given, and the potential flux $\partial\varphi/\partial x$ is considered zero at the channel walls.

To solve the momentum equation, the vertical and horizontal velocities in the channel walls are assumed to be zero. At the channel inlet, to eliminate the frictional and shape change effects, a parabolic velocity distribution with a maximum u_{in} in velocity is used, which represents a fully developed flow rate.

A fully developed condition is used for the velocity at the channel outlet.

$$\begin{cases} \text{inlet } x = 0 & \frac{u}{u_{in}} = \left[1 - \left(\frac{y}{H} \right)^2 \right], \quad v = 0 \\ \text{outlet } x = L & \partial u / \partial x = 0, \quad \partial v / \partial x = 0 \end{cases} \quad (15)$$

There is on the slip in the channel walls and the non-slip boundary condition is used ($u = v = 0$ in $y = \pm H$).

SMOOTH PARTICLE HYDRODYNAMICS METHOD

Formulation

The smooth particle hydrodynamics (SPH) method is used to solve the governing equations of the flow. SPH is a meshfree Lagrangian discretization scheme in which the continuous environment is discretized with a limited number of computational points. SPH uses an integral representation method in a weak form using a smoothing function with an interpolation domain called the support domain. If f is an arbitrary function in the support domain Ω , we can write [26]:

$$f(r) = \int_{\Omega} f(r') W(r - r', h) dr' \quad (16)$$

where r and r' are the position vectors and the sub-integral variable, W is called the smoothing or kernel function, and h is called the smooth length. Equation (16) can be approximated as a series of discretization in the domain Ω [26].

$$f(r) = \sum_{j=1} \omega_j f_j W(r - r', h) \quad (17)$$

In this study, the fifth-order Wendland kernel is used for the kernel function [27]. This recent research has shown that using this function causes the required computational accuracy and cost for most cases [26].

$$W(r, h) = 7/\pi h^2 \begin{cases} (1-s)^4(4s+1) & 0 \leq s \leq 1 \\ 0 & s \geq 1 \end{cases} \quad (18)$$

The first derivative of an arbitrary function f in the particle i can be approximated using the following general form [26].

$$\langle \nabla f \rangle_i = \sum_j G_{ij} (f_j - f_i) \quad (19)$$

Where j represents the neighboring particles of the particle i . f_j is the value of f in particle j , and G_{ij} is a weight function that shows the contribution of particle j to particle i . The values of G_{ij} are a function of the relative position vector of the neighbors of particle i , i.e. $r_{ij} = r_j - r_i$ [26].

$$G_{ij} = \omega_j B_i \cdot \nabla W_{ij} \quad (20)$$

Here ω_j is an infinitesimally small volume for a particle j and is defined as $\omega_j = m_j / \rho_j$, which in this study has a constant value for all SPH particles. Also, $W_{ij} = W(r_{ij}, h)$ is the smoothing or kernel function, which is a smoothed version of the Dirac Delta function and is a positive value for $r_{ij} = |r_{ij}| < h$ [20]. Tensor B is also the first-order normalizing tensor previously introduced by Bonet and Lok [29] to correct the first-order derivative of the kernel function [26].

$$B_i = -[\sum_j \omega_j \nabla W_{ij} \otimes r_{ij}]^{-1} \quad (21)$$

There are two main methods for approximating the second-order spatial derivative [30]. In the first method, another derivative of the first-order can be considered as [26]:

$$\langle \nabla \cdot \langle \nabla f \rangle \rangle_i = \sum G_{ij} \cdot (\langle \nabla f \rangle_j - \langle \nabla f \rangle_i) \quad (22)$$

By placing equation (19) in equation (22), gives [26]:

$$\langle \nabla \cdot \langle \nabla f \rangle \rangle_i = \sum_i \sum_k G_{ij} \cdot G_{ik} (f_k - f_j) - \sum_i G_{ij} (f_j - f_i) \quad (23)$$

Where the subtitles i , j , and k are the numerical indices of the particles, and k represents the neighbors j . Since in this design in Equation (23), addition is done twice on neighboring particles, it is referred to as the double addition scheme. In the second method, the second-order derivative uses the same pattern as the first derivative but with different weights [26].

$$\langle \nabla \cdot \nabla f \rangle_i = \sum_j Q_{ij} (f_j - f_i) \quad (24)$$

As described in [30], a second-order Laplacian consistent scheme can be expressed as [30]:

$$Q_{ij} = 2\hat{B}_i : \lambda_{ij} \quad (25)$$

Where [30],

$$\lambda_{ij} = \omega_j \left(\frac{e_{ij}}{r_{ij}} \otimes \nabla W_{ij} + S_{e2} \cdot B_i \cdot \nabla W_{ij} \right) \quad (26)$$

Where $e_{ij} = \frac{r_{ij}}{|r_{ij}|}$ and $S_{e2} = \sum_j \omega_j e_{ij} e_{ij} \nabla W_{ij}$. Also, \hat{B}_i is the normalized Laplacian tensor given by the following equation [30]:

$$\hat{B}_i : Z_i = I \quad (27)$$

Where in [30]:

$$Z_i = \sum_j \lambda_{ij} r_{ij} r_{ij} \quad (28)$$

In the present study, the second approach is used to calculate the second derivatives of the variables.

Density-based WCSPH for EOFs

First, the external potential field ϕ is solved.

$$\langle \nabla^2 \phi \rangle = 0 \quad (29)$$

To solve the Poisson-Boltzmann equation, the Taylor expansion of the \sinh function has been used. The main challenge in all numerical studies is the exponential nonlinearity of this term. Using the Taylor expansion, Equation (4), Poisson-Boltzmann equation, is modified and discretized as follows.

$$\sum_j 2\omega_j (\psi_i^{\mathfrak{R}+1} - \psi_j^{\mathfrak{R}+1}) \frac{e_{ij} \cdot (B_i \cdot \nabla W_{ij})}{|r_{ij}|} = \frac{2ze n_\infty}{\epsilon} \left[\sinh \left(\frac{ze \psi_i^{\mathfrak{R}}}{k_B T} \right) + \frac{ze}{k_B T} (\psi_i^{\mathfrak{R}+1} - \psi_i^{\mathfrak{R}}) \cosh \left(\frac{ze}{k_B T} \psi_i^{\mathfrak{R}} \right) \right] \quad (30)$$

The uppercase \mathfrak{R} shows the value calculated in the previous iteration, and the uppercase $\mathfrak{R} + 1$ shows the value in the new iteration. Inserting the Equation (9) in Equation (7) and rearrangements, it is deduced that:

$$\frac{1}{c^2} \frac{dp}{dt} = -\rho \nabla \cdot V \quad (31)$$

Here, a modified form of the algorithm is applied. The procedure is that first, the middle mean velocity field (\tilde{V}) is estimated without using the pressure term.

$$\rho \left(\frac{\tilde{V} - V^n}{\Delta t} \right) = \mu \langle \nabla^2 V^n \rangle + \rho g + \left\langle \frac{\rho_f E}{\rho} \right\rangle \quad (32)$$

Combining Equation (32) and Equation (31), the following equation can be deduced:

$$V^{n+1} = \tilde{V} - \left\langle \frac{\nabla P^n}{\rho} \right\rangle \quad (33)$$

Then, by applying divergence to Equation (33) and placing it in Equation (31), the new pressure is calculated by the following equation.

$$\frac{P^{n+1} - P^n}{\Delta t} = -\rho c^2 \left(\langle \Delta \cdot \tilde{V} \rangle - \Delta t \frac{\langle \nabla \cdot \nabla P^n \rangle}{\rho} \right) \quad (34)$$

In the next step, the new velocity is calculated using the following equation.

$$V^{n+1} = \tilde{V} - \Delta t \frac{\langle \nabla P^{n+1} \rangle}{\rho} \quad (35)$$

Equations (32) to (35) form a predictive-corrective scheme similar to the methods explained in references [31] and [32] with some corrections and mathematical manipulations. The main difference here is that the density is assumed to be constant. This algorithm dramatically alters the extreme fluctuations of the standard method of weakly compressible smooth particle hydrodynamics. Finally, the new position of the particles is calculated as follows:

$$r^{n+1} = r^n + V^{n+1} \Delta t \quad (36)$$

If the mass transfer equation needs to be solved, Equation (10) is solved as follows.

$$c^{n+1} = c^n + \alpha \langle \nabla^2 c \rangle^n \Delta t \quad (37)$$

According to the idea of Shadloo et al. [33] at the end of each time step, all internal particles are displaced according to the following equation.

$$\Delta r_i = \epsilon V_i \Delta t \sum_j \left(\frac{d_0}{r_{ij}} \right)^3 e_{ij} \quad (38)$$

Where d_0 is the distance of the initial particles (from the reference point based on the Lagrangian concept) and ϵ can take a value between 0 and 0.1.

After placing the particle in the new position, it is necessary to correct the values of other field variables as well. Hence, the expansion of the first sentence of the Taylor series is used as follows for other variables.

$$\Delta \varphi_i = \Delta r_i \cdot \langle \nabla \varphi \rangle_i \quad (39)$$

$$\Delta \psi_i = \Delta r_i \cdot \langle \nabla \psi \rangle_i \quad (40)$$

$$\Delta V_i = \Delta r_i \cdot \langle \nabla V \rangle_i \quad (41)$$

$$\Delta P_i = \Delta r_i \cdot \langle \nabla P \rangle_i \quad (42)$$

$$\Delta C_i = \Delta r_i \cdot \langle \nabla C \rangle_i \quad (43)$$

Dummy particles are used to apply boundary conditions. These particles have been used according to the design of Lee et al. [34]. These particles have a velocity equal to the velocity of the corresponding wall particles and also, for the stationary wall, in the direction perpendicular to the wall, they have the same pressure equal to that of the wall particle. A numerical code has been implemented to solve EOFs based on the density-based WCSPH method. Code developed to solve EOFs, solves the Laplace, Poisson Boltzmann equation based on the particle method (Lagrangian approach). The effect of EOF is solved by entering the momentum equation and applying the algorithm described in Table 1. This code eliminates the density

fluctuations that can cause numerical errors using a new time algorithm with velocity and pressure coupling.

GEOMETRY OF CASE STUDY

Fig. 1 shows the proposed geometry for the Electroosmotic microchannel. This two-dimensional microchannel has a height of $2H$ and a length of L . It is exposed to the external electric field E_0 at both ends. The microchannel consists of nonuniform charge distribution in the walls and its length is divided into 7 equal parts. Red lines show the negative charge $\psi_n = -|\zeta|$ with length $\frac{1}{7}L$, and blue lines show the positive charge $\psi_p = +|\zeta|$ with length $\frac{1}{7}L$. Also, the patches, $\psi_0 = 0$ are without charge and have a length of $\frac{2}{7}L$ at the inlet and outlet of the channel so that the mid-length of charged patches is $\frac{1}{7}L$.

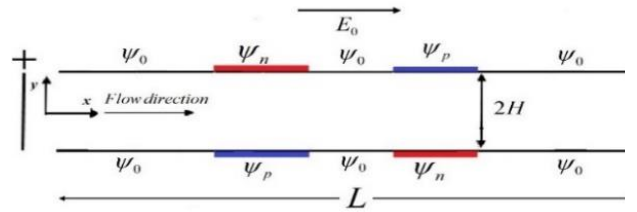


Fig. 1. The modeled two dimensional electroosmotic microchannel

Table 1

summarizes the computational algorithm

```

for each time-step  $n$  do
  find the neighboring particles;
  for each particle  $i$  do
    compute  $\varphi$  using Eq. (29) ;
    compute  $\psi$  using Eq. (30) ;
    compute  $\tilde{V}$  using Eq. (32);
  end for
  for each internal particle  $i$  do
    compute  $P^{n+1}$  using Eq. (34);
  end for
  update pressure of wall particles;
  for each internal particle  $i$  do
    compute  $V^{n+1}$  using Eq. (35);
  end for
  for each internal particle  $i$  do
    compute  $r^{n+1}$  using Eq. (36);
  end for
  if mass transfer is active then
    calculate  $c^{n+1}$  using Eq. (37);
  end if
  for each internal particle  $i$  do
    shift the position by  $\Delta r_i$  evaluated from Eq. (38);
    correct EDL potentials, external potential,
    velocity, pressure, concentration using Eqs. (39) to (43);
  end for
end for

```

The microchannel is filled with an electrolyte solution assumed to be a Newtonian fluid with constant properties. The parameters and constants used in this problem are given in Table 2.

Table 2

Specifications of parameters and constants used in the modeled electroosmotic microchannel

Fluid density	ρ	1000 (kg/m ³)
Permittivity of vacuum	ϵ_0	8.854×10^{-12} (F/m)
Dielectric constant of the medium	ϵ_r	78.5
Valence	z	1
Charge of an electron	e	1.6×10^{-19} C
Boltzmann constant	k_b	1.38×10^{-23} J/k
Absolute temperature	T	300 K
External electric potential at the inlet	φ_{in}	10 v
External electric potential at the outlet	φ_{out}	0 v
Microchannel Height	H	10 μ m
Microchannel Length	L	140 μ m
Diffusion Coefficient	D	10^{-12} (m ² /s)
Debye Length	λ_D	2μ m

VALIDATION OF RESULTS AND INDEPENDENCE OF SOLUTION FROM THE PARTICLE

The accuracy of the program has been validated with a model that has already been solved analytically and numerically by Dutta and Beskok [3]. This model includes a two-dimensional microchannel with a height of $2H$ and a length of $L_1 + L_2 + L_3$. The length of the channel is divided into three parts. According to Fig. 2, the middle part contains a material with some electroosmotic effects, while these effects are neglected for the beginning and end of the channel. The channel is filled with a Newtonian electrolyte fluid of constant density and viscosity. The height of the channel is $H = 10\mu$ m and the length of each part of the channel is $L_1, L_2, L_3 = 31\mu$ m. The geometry of this numerically modeled problem is shown in Figure 2.

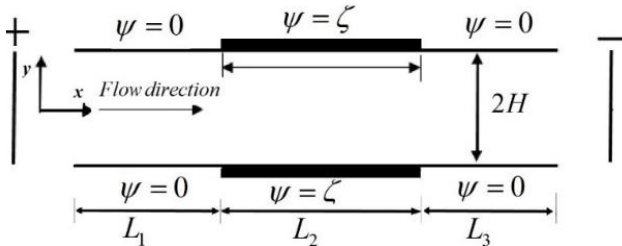


Fig. 2. Modeling of a two dimensional electroosmotic microchannel adopted from reference [3]

Velocity components in x and y directions are normalized with reference velocity U_{ref} (i.e. $U = u/U_{ref}$ and $V^* =$

v/U_{ref}), the electroosmotic potential is normalized with ζ (i.e. $\psi^* = \psi/\zeta$) and the coordinates in the longitudinal and transverse directions are normalized with respect to half-height of the channel H (i.e. $\xi = x/H$ and $\eta = y/H$) and the pressure P is divided by $\mu U_{ref}/H$ to obtain P^* (i.e. $P^* = PH/\mu U_{ref}$). The reference velocity U_{ref} is calculated based on the reference Reynolds $Re_{ref} = \frac{\rho U_{ref} 2H}{\mu}$. Here, the specified value of $Re_{ref} = 0.005$ is dimensionless. Fig. 3 shows the axial dimensionless velocity in terms of dimensionless width at the center of the channel, i.e. $\xi = 4.5$ for $U_{in} = 2$. U_{in} is dimensionless. input velocity (u_{in}) which is divided reference velocity (i.e. $U_{in} = u_{in}/U_{ref}$). The compatibility of the solution results with the reference solution [3] is evident. Also, to investigate the convergence and solubility independence of the particle, the velocity distributions for three different particle distances $\Delta x = 4 \times 10^{-7}$, $\Delta x = 2.5 \times 10^{-7}$ and $\Delta x = 2 \times 10^{-7}$ have been examined. Considering these three particle distances, Fig. 4 shows the numerical solution values of the dimensionless velocity distribution in the middle of the channel with $U_{in} = 2$. These results show the velocity convergence at $\Delta x = 2 \times 10^{-7}$ as compared to those results given in the reference solution [3].

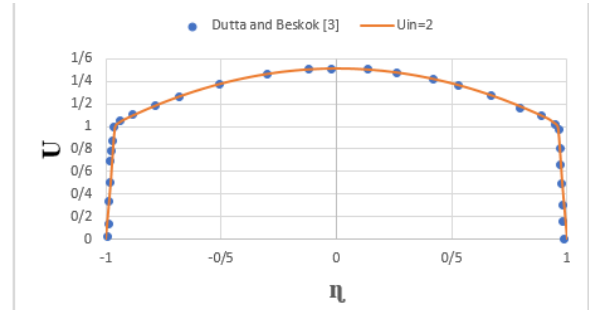


Fig. 3. Dimensionless velocity distribution in the center of the channel. These numerical results are compared with those given in the reference [3].

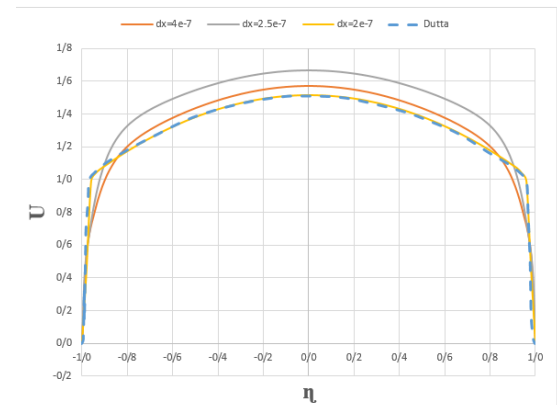


Fig. 4. Dimensionless velocity distribution in the center of the channel for $U_{in} = 2$ for the three particle spacing $\Delta x = 4 \times 10^{-7}$, $\Delta x = 2.5 \times 10^{-7}$ and $\Delta x = 2 \times 10^{-7}$ and comparison with reference solution [3].

RESULTS AND DISCUSSION

The geometry shown in Fig. 1 is solved numerically. For a dimensionless solution, as in the steps validating the results, the parameters are dimensionless and Reynolds's base is $Re_{ref} = 0.005$. To investigate the effect of surface zeta potential on the flow, the two potentials $\zeta = -100\text{ mV}$ and $\zeta = -25\text{ mV}$ have been compared. Maximum velocity at the inlet of the microchannel is considered as $u_{in} = 0.15\text{ mm/s}$. Fig. 5 shows the dimensionless horizontal velocity contour for two potential values. A particle representation is used to represent the contour, and the arrangement of the particles is evident in the figure.

As can be seen in Fig. 5, for each potential stream, positive and negative velocity zones are created. The EOF is the force that results from the interaction of an external electric field with EDL. Considering the direction of the externally applied electric field from the upstream of the microchannel to the downstream, a thrust force is produced. This force is in the direction of the applied pressure gradient inside the EDL adjacent to the surfaces with negative zeta potential (shown in red in Fig. 1). A thrust force is also generated in contrast to the applied pressure gradient near the positively charged surfaces (indicated by the blue color in Fig. 1). The interaction of these EOFs with the bulk flow (A bulk flow is a flow that is obtained due to pressure difference and is not affected by the potential of the surface) in the center of the channel due to the applied pressure gradient (that moves in a positive axial direction) leads to the formation of regional circulation zones that are symmetrically adjacent to the heterogeneous charged surfaces. Although rotational regions are obtained in both shapes, the strength of this rotational flow is different in two shapes. Fig. 5 shows that the maximum reverse flow is approximately 4 times faster than the reference velocity, At the same time in the bottom figure, it is approximately equal to the reference velocity and shows that for higher potential values the rotational regions are wider and stronger.

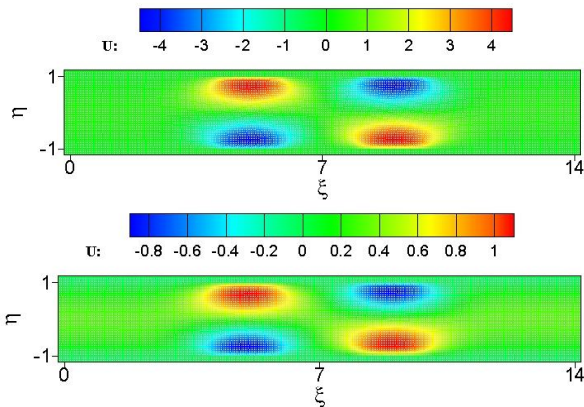


Fig. 5. Dimensionless horizontal velocity contours for zeta potential. Top figure is for $\zeta = -100\text{ mV}$ and bottom figure is for $\zeta = -25\text{ mV}$

In Fig. 6, there are larger rotational regions in the upper figure than in the lower figure, which is due to the fact that the higher potential created a larger level of EOFs, which resulted in larger rotational regions. The rotating zones force the flow of the bulk to pass through a smaller cross-sectional area, which is shown in Fig. 6. The narrower the passage, the longer and stronger the vortex. In other words, as shown in

Fig. 7, when the area above the vortices is smaller. The length of the vortex is longer and the vortex is stronger. As can be seen from the figure, the direction of the initial vortex is clockwise and that of the downward vortex is anticlockwise because the heterogeneous distribution of charge at the beginning of the microchannel is such that the clockwise vortex can be created. It is also illustrated in Fig. 6 that the stream lines, like the microchannel input, are parallel and the transverse velocity is eliminated, which is evidence of the development conditions.

In Fig. 7, the dimensionless velocity profiles are drawn along the horizontal direction for the two potentials $\zeta = -100\text{ mV}$ and $\zeta = -25\text{ mV}$ in two sections $\xi = 5$ and $\xi = 10$, respectively. The velocity profile at $\xi = 5$ has a higher value for more potential flow, and the velocity profile has positive values near the top surface and negative values near the bottom surface, which indicates the vortex flow formed at this section. The symmetry in the velocity profile is also due to the symmetry in surface potential, which produces the same EOFs but in opposite directions. By comparing the velocity at $\zeta = -100\text{ mV}$, a higher potential flow develops the larger values of the velocity than that of the lower potential flow. It can also be seen in Fig. 7, the value of the velocity profile in $\zeta = -100\text{ mV}$ is almost 4 times $\zeta = -25\text{ mV}$.

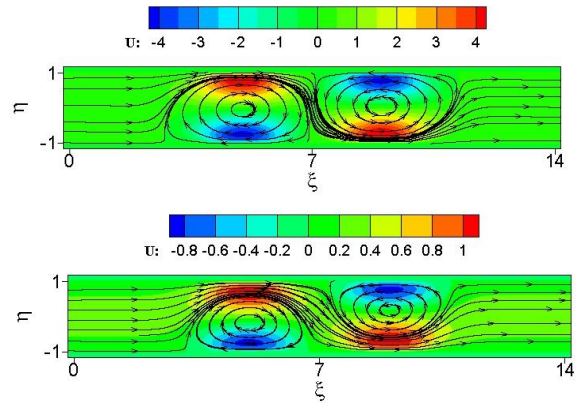


Fig. 6. Dimensionless streamlines. The top figure shows the streamlines for $\zeta = -100\text{ mV}$ and the bottom figure is for $\zeta = -25\text{ mV}$

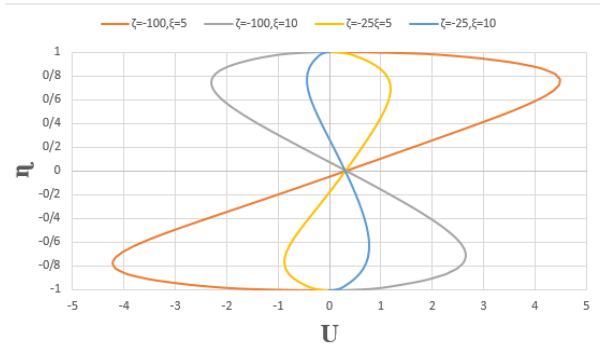


Fig. 7. Dimensionless velocity profiles for the two potentials $\zeta = -100\text{ mV}$ and $\zeta = -25\text{ mV}$ in the two sections $\xi = 5$ and $\xi = 10$

Fig. 8 shows the concentration distribution for the two potentials $\zeta = -100\text{ mV}$ and $\zeta = -25\text{ mV}$. As shown in the figure, Fluid shown in red color ($c = 1$) enter the microchannel from the upper half and fluid shown in blue color ($c = 0$) enter the microchannel from the lower half. All the physical properties of two fluids are assumed to be similar, and the two fluids differ only in one scalar property (concentration). In the upper half of the microcurrent, a concentration of 1 is applied in the upper half of microchannel and a concentration of zero is applied in the lower half of microchannel. The ideal mixing ($c = 0.5$) is shown in green. The rotational zones created near the heterogeneous surfaces produce a reverse electroosmotic force that causes the disturbance of the species to increase with the convection and diffusion mechanism. Larger vortexes produce stronger convection effects, which in turn lead to increase the species mixing and cause higher mixing efficiency. As shown in Fig. 8, the green areas are greater at greater potential, indicating better species mixing.

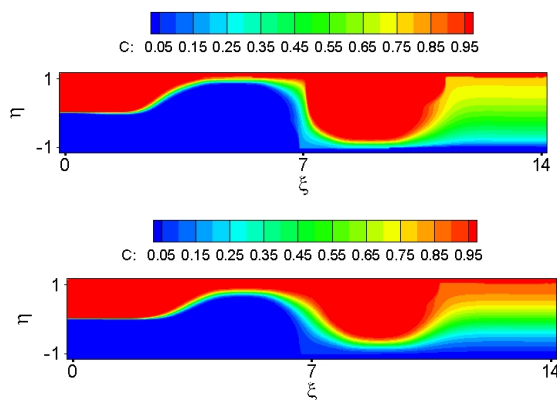


Fig. 8. Concentration distribution. Top figure is for $\zeta = -100\text{ mV}$ and bottom figure is for $\zeta = -25\text{ mV}$

Fig. 9 shows the mixing efficiency of the two potentials $\zeta = -100\text{ mV}$ and $\zeta = -25\text{ mV}$. As shown in the figure, the mixing efficiency has increased by about 40% at the microchannel outlet, which means that the species exiting the microchannel with greater potential have more mixing.

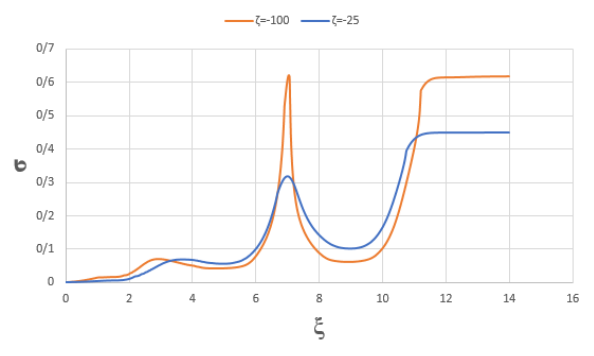


Fig. 9. The mixing efficiency. The top figure is for $\zeta = -100\text{ mV}$ and the bottom figure is for $\zeta = -25\text{ mV}$

CONCLUSION

Two-dimensional microchannels with asymmetric charge distribution under the simultaneous effects of pressure gradient and electroosmotic force have been studied. Flow characteristics are obtained by solving the Poisson Boltzmann and Navier Stokes equations based on the Lagrangian approach and using the density-based WCSPH. In this paper, numerical code based on density-based WCSPH method has been used to eliminate fluctuations and ill functions. Distributing the potential charge with opposite signs on the surface creates a reverse electroosmotic force, resulting in rotational zones in the flow. This type of charge distribution is very efficient for mixing purposes by creating rotational flows in the microchannel. The results show that the increase in zeta potential produces more intense velocity fields and consequently stronger vortexes are created. As the zeta potential increases, the potential of the EDL increases, which produces larger electroosmotic forces and increases the mixing efficiency.

REFERENCES

- [1] Capretto L, Cheng W, Hill M, Zhang X. Micromixing within microfluidic devices. *Microfluidics*: Springer. 2011; 27-68.
- [2] Liu S, Dasgupta PK. Electroosmotically pumped capillary flow-injection analysis: valve-based injection systems and sample throughput. *Analytica chimica acta*. 1993; 283(2): 739-745.
- [3] Dutta P, Beskok A, Warburton TC. Numerical simulation of mixed electroosmotic/pressure driven microflows. *Numerical Heat Transfer: Part A: Applications*. 2002; 41(2): 131-148.
- [4] Hu J, Chao CY. A study of the performance of microfabricated electroosmotic pump. *Sensors and Actuators A: Physical*. 2007;135(1):273-282.
- [5] Patankar NA, Hu HH. Numerical simulation of electroosmotic flow. *Analytical Chemistry*. 1998; 70(9): 1870-1881.

- [6] Ajdari A. Electro-osmosis on inhomogeneously charged surfaces. *Physical Review Letters*. 1995; 75(4): 755.
- [7] Ren L, Li D. Electroosmotic flow in heterogeneous microchannels. *Journal of colloid and interface science*. 2001; 243(1): 255-261.
- [8] Erickson D, Li D. Influence of surface heterogeneity on electrokinetically driven microfluidic mixing. *Langmuir*. 2002; 18(5): 1883-1892.
- [9] Yariv E. Electro-osmotic flow near a surface charge discontinuity. *Journal of Fluid Mechanics*. 2004; 521: 181.
- [10] Tian F, Li B, Kwok DY. Tradeoff between mixing and transport for electroosmotic flow in heterogeneous microchannels with nonuniform surface potentials. *Langmuir*. 2005; 21(3): 1126-1131.
- [11] Lee JS, Ren CL, Li D. Effects of surface heterogeneity on flow circulation in electroosmotic flow in microchannels. *Analytica Chimica Acta*. 2005; 530(2): 273-282.
- [12] Luo WJ, Yarn KF, Hsu SP. Analysis of electrokinetic mixing using AC electric field and patchwise surface heterogeneities. *Japanese journal of applied physics*. 2007; 46(4R): 1608.
- [13] Bhattacharyya S, Nayak A. Electroosmotic flow in micro/nanochannels with surface potential heterogeneity: An analysis through the Nernst–Planck model with convection effect. *Colloids and Surfaces A: Physicochemical and Engineering Aspects*. 2009; 339(1-3): 167-177.
- [14] Bhattacharyya S, Nayak A. Combined effect of surface roughness and heterogeneity of wall potential on electroosmosis in microfluidic/nanofluidic channels. *Journal of Fluids Engineering*. 2010; 132(4).
- [15] Sun CI, Shie SS. Optimization of a diverging micromixer driven by periodic electroosmotics. *Microsystem technologies*. 2012; 18(9-10): 1237-1245.
- [16] Jain M, Nandakumar K. Optimal patterning of heterogeneous surface charge for improved electrokinetic micromixing. *Computers & Chemical Engineering*. 2013; 49: 18-24.
- [17] Sadeghi A, Azari M, Chakraborty S. H₂ forced convection in rectangular microchannels under a mixed electroosmotic and pressure-driven flow. *International Journal of Thermal Sciences*. 2017; 122: 162-171.
- [18] Cheng Y, Jiang Y, Wang W. Numerical simulation for electro-osmotic mixing under three types of periodic potentials in a T-shaped micro-mixer. *Chemical Engineering and Processing-Process Intensification*. 2018; 127: 93-102.
- [19] Gaikwad HS, Mondal PK, Basu DN, Chimres N, Wongwises S. Analysis of the effects of Joule heating and viscous dissipation on combined pressure-driven and electrokinetic flows in a two-parallel plate channel with unequal constant temperatures. *Proceedings of the Institution of Mechanical Engineers, Part E: Journal of Process Mechanical Engineering*. 2019; 233(4): 871-879.
- [20] Azari M, Sadeghi A, Chakraborty S. Graetz problem for combined pressure-driven and electroosmotic flow in microchannels with distributed wall heat flux. *International Journal of Heat and Mass Transfer*. 2019; 128: 150-160.
- [21] Kazemi Z, Rashidi S, Esfahani JA. Effect of flap installation on improving the homogeneity of the mixture in an induced-charge electrokinetic micromixer. *Chemical Engineering and Processing: Process Intensification*. 2017; 121: 188-197.
- [22] Saravani MS, Kalteh M. Heat transfer investigation of combined electroosmotic/pressure driven nanofluid flow in a microchannel: Effect of heterogeneous surface potential and slip boundary condition. *European Journal of Mechanics-B/Fluids*. 2020; 80: 13-25.
- [23] Qaderi A, Jamaati J, Bahiraei M. CFD simulation of combined electroosmotic-pressure driven micromixing in a microchannel equipped with triangular hurdle and zeta-potential heterogeneity. *Chemical Engineering Science*. 2019; 199: 463-477.
- [24] Masliyah JH, Bhattacharjee S. *Electrokinetic and colloid transport phenomena*: John Wiley & Sons; 2006.
- [25] Liu GR, Liu MB. *Smoothed particle hydrodynamics: a meshfree particle method*: World scientific; 2003.
- [26] Wendland H. Piecewise polynomial, positive definite and compactly supported radial functions of minimal degree. *Advances in computational Mathematics*. 1995; 4(1): 389-396.
- [27] Gingold RA, Monaghan JJ. Smoothed particle hydrodynamics: theory and application to non-spherical stars. *Monthly notices of the royal astronomical society*. 1977; 181(3): 375-389.
- [28] Bonet J, Lok T-S. Variational and momentum preservation aspects of smooth particle hydrodynamic formulations. *Computer Methods in applied mechanics and engineering*. 1999; 180(1-2): 97-115.
- [29] Fatehi R, Manzari M. A remedy for numerical oscillations in weakly compressible smoothed particle hydrodynamics. *International Journal for Numerical Methods in Fluids*. 2011; 67(9): 1100-1114.
- [30] Sefid M, Fatehi R, Shamsoddini R. A modified smoothed particle hydrodynamics scheme to model the stationary and moving boundary problems for Newtonian fluid flows. *Journal of Fluids Engineering*. 2015; 137(3).
- [31] Shamsoddini R, Sefid M, Fatehi R. Lagrangian simulation and analysis of the micromixing phenomena in a cylindrical paddle mixer using a

- modified weakly compressible smoothed particle hydrodynamics method. *Asia-Pacific Journal of Chemical Engineering*. 2015; 10(1): 112-124.
- [33] Shadloo MS, Zainali A, Sadek SH, Yildiz M. Improved incompressible smoothed particle hydrodynamics method for simulating flow around bluff bodies. *Computer methods in applied mechanics and engineering*. 2011; 200(9-12): 1008-1020.
- [34] Lee ES, Moulinec C, Xu R, Violeau D, Laurence D, Stansby P. Comparisons of weakly compressible and truly incompressible algorithms for the SPH mesh free particle method. *Journal of computational Physics*. 2008; 227(18): 8417-8436.